Pharmacological and Metabolic Parameters of [^{18}F]Flubrobenguane in Clinical Imaging Populations

Braeden A. Mair BSc,[1,2] Jason G. E. Zelt MD, PhD,[2,3] Kirabo Nekesa BSc,[1,2] Zacharie Saint-Georges BSc,[2,4,5] Katie Dinelle MSc,[5] Myriam Adi,[1,2] Simon Robinson PhD,[6] Lisa M. Mielniczuk MD,[2] Jakov Shlik MD, PhD,[5,7] Rob S. Beanlands MD,[2] Robert A. deKemp PhD,[2] and Benjamin H. Rotstein PhD[1,2,8]

[1] Department of Chemistry and Biomolecular Sciences, University of Ottawa, Ottawa, Canada
[2] University of Ottawa Heart Institute, Ottawa, Canada
[3] Department of Medicine, Faculty of Medicine, University of Ottawa, Ottawa, Canada
[4] Department of Cellular and Molecular Medicine, University of Ottawa, Ottawa, Canada
[5] The University of Ottawa Institute of Mental Health Research at The Royal, Ottawa, Canada
[6] Lantheus Medical Imaging, Inc, North Billerica, MA, USA
[7] Department of Psychiatry, University of Ottawa, Ottawa, Canada
[8] Department of Biochemistry, Microbiology and Immunology, University of Ottawa, Ottawa, Canada

Corresponding Authors:
Benjamin H. Rotstein, PhD
Email: benjamin.rotstein@uottawa.ca
University of Ottawa Heart Institute
40 Ruskin Street, Ottawa, ON, Canada, K1Y 4W7
ORCID: 0000-0001-9707-9357

Robert A. deKemp, PhD
Email: radekemp@ottawaheart.ca
University of Ottawa Heart Institute
40 Ruskin Street, Ottawa, ON, Canada, K1Y 4W7
ORCID: 0000-0001-9136-5563

Disclosures:

R.D.K. receives royalties from Rubidium PET technologies licensed to Jubilant Radiopharma and INVIA Medical Solutions; and received unrestricted research grant funding or honoraria from Siemens Molecular Imaging, IONETIX and Jubilant Radiopharma. R.S.B. has received honoraria and grants from GE HealthCare, Lantheus Medical Imaging, Inc, and Jubliant Draximage not related to this work. The other authors report no disclosures.

Funding:

This study was supported by the Heart and Stroke Foundation of Canada, the Cardiovascular Network of Canada (CANet), and an Ontario Early Researcher Award to B.H.R. This project was also funded by a university-industry partnership grant (RE07-021) from the Ontario Research Fund, Lantheus Medical Imaging, Inc, the University Medical Research Fund, and a Faculty of Medicine Translational Research Grant. B.A.M. is supported by the Natural Science and Engineering Research Council of Canada (NSERC PGS-D). J.G.E.Z. and Z.S. are supported by the Vanier Canada Graduate Scholarship Program. R.S.B. is supported in part by an University of Ottawa Distinguished Chair in Cardiac Imaging Research.

ABSTRACT

Background: Cardiac sympathetic nervous system molecular imaging has demonstrated prognostic value. Compared with *meta*-[^{11}C]hydroxyephedrine, [^{18}F]flubrobenguane (FBBG) facilitates reliable estimation of SNS innervation using similar analytical methods and possesses a more convenient physical half-life. The aim of this study was to evaluate pharmacokinetic and metabolic properties of FBBG in target clinical cohorts.

Methods: Blood sampling was performed on 20 participants concurrent to FBBG PET imaging (healthy = NORM, non-ischemic cardiomyopathy = NICM, ischemic cardiomyopathy = ICM, post-traumatic stress disorder = PTSD). Image-derived blood time-activity curves were transformed to plasma input functions using cohort-specific corrections for plasma protein binding, plasma-to-whole blood distribution, and metabolism.

Results: The plasma-to-whole blood ratio was 0.78 ± 0.06 for NORM, 0.64 ± 0.06 for PTSD and 0.60 ± 0.14 for (N)ICM after 20 minutes. 22 ± 4% of FBBG was bound to plasma proteins. Metabolism of FBBG in (N)ICM was delayed, with a parent fraction of 0.71 ± 0.05 at 10 minutes post-injection compared to 0.53 ± 0.03 for PTSD/NORM. While there were variations in metabolic rate, metabolite-corrected plasma input functions were similar across all cohorts.

Conclusions: Rapid plasma clearance of FBBG limits the impact of disease-specific corrections of the blood input function for tracer kinetic modeling.

Key Words: flubrobenguane, PET, fluorine-18, metabolism, sympathetic nervous system

Abbreviations:

FBBG	[^{18}F]Flubrobenguane
HED	*Meta*-[^{11}C]hydroxyephedrine
HF	Heart failure
ICM	Ischemic cardiomyopathy
NET	Norepinephrine transporter
NICM	Non-ischemic cardiomyopathy
PET	Positron emission tomography
PPB	Plasma protein binding
PTSD	Post-traumatic stress disorder
SNS	Sympathetic nervous system

INTRODUCTION

[^{18}F]Flubrobenguane, or *N*-[3-bromo-4-(3-[^{18}F]fluoropropoxy)benzyl]guanidine (FBBG, also known as LMI1195),[1] is a recently developed radiotracer designed for imaging of the cardiac sympathetic nervous system (SNS) using positron emission tomography (PET). Its uptake into myocardium, mediated by the norepinephrine transporter (NET), is diminished in patients with ICM as a result of progressive denervation.[2] The two most prominent SNS molecular imaging agents are *meta*-[^{123}I]iodobenzylguanidine (mIBG) used in gamma scintigraphy and single-photon emission computed tomography (SPECT), and *meta*-[^{11}C]hydroxyephedrine (HED) used in PET. These radiotracers have shown utility in cardiac imaging clinical trials, assisting in mortality prognostication, evaluation of arrhythmias and in identifying highest risk for sudden cardiac death in patients suffering from cardiomyopathies.[3–5] Non-invasive SNS imaging offers considerable potential for cardiac care, although limitations exist with the current methods.

Despite the availability of mIBG, suboptimal image quality and semi-quantification[6] have limited its utility in cardiac SNS imaging. Furthermore, while PET offers superior image quality over SPECT,[5] the short half-life of carbon-11 (20.4 min) in HED limits clinical access and wider distribution. FBBG is a benzylguanidine similar to mIBG but carries a fluorine-18 nuclide for PET imaging with a convenient 110-minute half-life that can support wider availability, multi-site clinical trials, and quantitative imaging protocols. FBBG shares similar biodistribution profiles to mIBG in preclinical models.[1,7,8] We explored a similar comparison with HED, and demonstrated that FBBG and HED provide equivalent regional quantitative distribution in patient cohorts with and without ischemic cardiomyopathy.[2,9] Additionally, a first-in-human study reported on dosimetry, biodistribution and safety in 12 healthy subjects.[10]

Accurate quantification of NET distribution using kinetic modeling requires a set of corrections, including for blood metabolites, to obtain accurate parent plasma input functions. Sinusas *et al.* reported such measurements in healthy volunteers,[10] which we applied in our initial analysis of FBBG imaging in cardiomyopathy patients.[2] However, these corrections may not be applicable to all patients, particularly those with dysfunctional NET activity.[11] To this end, we have further investigated the blood-based distribution and metabolic profiles of FBBG in relevant clinical imaging populations.

The aims of this study were to determine the plasma metabolite and distribution profiles needed to obtain accurate input functions for FBBG in patients with non-ischemic cardiomyopathy (NICM), ischemic cardiomyopathy (ICM), and in healthy volunteers (NORM). Additionally, we included patients with post-traumatic stress disorder (PTSD) as part of ongoing research into a group at elevated risk of heart failure.[12] Beginning with an image-derived blood input function of the radiotracer, we determined the amount of freely available parent fraction (non-metabolized FBBG) in plasma throughout our PET data acquisition. To access this function, we observed the ratio of activity in the plasma compared to whole blood, the binding of FBBG to plasma proteins, and the metabolism of the parent compound in plasma over time.

METHODS

Patient Population

We previously reported FBBG cardiac imaging in ischemic and nonischemic cardiomyopathy patients and healthy volunteers.[2] Data reported herein were collected both from a subsample of the previously reported cohort as well as additional subjects recruited using the same criteria. Recruitment methodology for patients with PTSD can be found in the Supplemental Information. Characteristics of imaging subjects can be found in **Table S1**. The study was approved by the Ottawa Health Science Network Research Ethics Board. All patients provided informed consent.

PET Imaging and Blood Collection

Patients underwent 40-minute or 60-minute dynamic FBBG PET imaging in a supine position while awake in a GE Discovery 690 PET-CT scanner (Waukesha, WI) or Siemens mMR PET-MR scanner (Knoxville, TN). The radiosynthesis of FBBG was performed as previously described.[1,10,13] A bolus of 3 MBq/kg FBBG (followed by a 10 mL saline push) was administered intravenously. Venous blood (>2 mL) was collected into heparinized tubes through a cannula placed in a vein in the antecubital fossa of the opposite arm to injection at a series of nominal timepoints (0.5, 1, 2, 5, 10, 20, 30, 40, 60 min).

Plasma Protein Binding

Tracer binding to plasma proteins is assumed to occur instantaneously following injection and to remain stable over the course of imaging. The free fraction in plasma (f_P) was determined using ultracentrifugation. f_P was calculated by subtracting the bound fraction from 1. More details on the methodology can be found in the Supplemental Information.

Plasma-to-Whole Blood Ratio

Tracer uptake into red blood cells follows a biexponential time-course and affects concentration in plasma available for exchange with target tissues.[14] To account for this time-dependent effect, activity in aliquots of plasma and whole blood were compared to derive a plasma-to-whole blood concentration ratio (PBR). The methodology is further described in the Supplemental Information.

A curve describing the cohort-specific plasma-to-whole blood ratio over time was determined by fitting to the function shown in **Equation 1**:

$$PBR(t) = Ae^{-mt^2} + B(1 - e^{-nt}) \quad (1)$$

Where *t* is the blood sample time in minutes, and *A*, *B*, *m,* and *n* are function parameters derived for each cohort. Area under the curve (AUC) was calculated using GraphPad Prism 9.0 (La Jolla, CA), following the trapezoid rule.

Plasma Metabolites

Samples were prepared similarly to the HPLC protocol described elsewhere[10] and in the Supplemental Information. A solid-phase extraction method to separate FBBG from metabolites was validated against patient samples also analyzed by HPLC; results were equivalent by both methods. Protein-free plasma samples were loaded onto a Sep-Pak Light C18 cartridge and washed with increasing concentrations of acetonitrile in water (0%, 10%, 20%, 20%, 30%, 70%, 100%, 100%). Each sample and residual activity on the cartridge was then assayed on a γ-counter. Polar metabolites were eluted with ≤30% acetonitrile, whereas the parent compound was eluted with ≥70%. The resulting collected activity was summed to determine the fraction of parent compound in plasma.

A curve describing the cohort-specific unaltered parent FBBG fraction (PF) over time was determined by fitting to **Equation 2**:

$$PF(t) = 1 - e^{-\frac{\tau}{t}} \quad (2)$$

where *t* is the blood sample time in minutes, and τ is a time constant describing the rate of conversion to metabolites in each cohort.

Metabolite-Corrected Image-Derived Plasma Input Function

Dynamic PET images were analyzed with Hybrid Viewer PDR 6.1.2 software (Hermes Medical Solutions). Spherical regions of interest were drawn in the left atrial cavity and the resulting whole-blood time-activity curves, $C_{WB}(t)$, were recorded (**Figure 1**). To account for small variations in tracer arrival time, a gamma variate function was fit to the bolus first-pass data (0–2 min), and the $C_{WB}(t)$ curves were resampled to unit area with the peak centered at 1 minute post-scan start.

For each scan, a final image-derived input function was then calculated according to **Equation 3**, representing the concentration of unaltered parent FBBG in arterial plasma:

$$C_{FP}(t) = C_{WB}(t) \times PBR(t) \times PF(t) \times f_P \quad (3)$$

where *t* is the dynamic image sampling time in minutes. Area under the curve (AUC) was then calculated as the time frame-weighted activity.

Statistics

Data are reported as a mean with standard deviation or mean with 95% confidence interval. Metabolic time constants, PBR(t) constants and AUC values were compared between groups using one-way ANOVA. Curve fitting, statistical analysis and graphical representation were performed using GraphPad Prism.

RESULTS

Plasma Protein Binding

Among patient cohorts (NICM = 5, ICM = 5, NORM = 5, PTSD = 5), there were 4 NICM, 4 ICM, 2 NORM and 2 PTSD data sets available. The remaining participants were not included due to missing blood sampling prior to radiotracer administration. The bound fraction was found to be 23 ± 4% in NICM, 22 ± 1% in ICM, 17 ± 5% in NORM, and 27 ± 5% in PTSD. The overall mean value was 22 ± 4%, with no significant difference between patient groups (ANOVA, $p > 0.05$) as shown in **Figure 2A**.

Plasma-to-Whole Blood Ratio

The plasma-to-whole blood ratio reached a maximum of 1.4 ± 0.1 early after injection before settling to 0.78 ± 0.1 for NORM, 0.64 ± 0.1 for PTSD and 0.60 ± 0.1 for the cardiomyopathy cohorts ((N)ICM) at 20 minutes post-injection (**Figure 2B**). There was no significant difference in AUC between cohorts (ANOVA, $p > 0.05$). Fits were derived according to the formula described by **Equation 1** and plotted (**Figure S1**). Parameters *A*, *B*, *m*, and *n* were compared; significant differences were found in parameter *n* between ICM and other cohorts (**Table 1**, $p = 0.038$ vs NORM, $p = 0.002$ vs NICM, $p = 0.010$ vs PTSD).

Plasma Metabolites

The parent fraction was determined for each of the cohorts (**Figure 2C**). After 10 minutes, the parent fraction was 0.71 ± 0.05 and 0.53 ± 0.03 in the (N)ICM and healthy/PTSD cohorts respectively. After 30 minutes, 0.32 ± 0.06 and 0.24 ± 0.02 unaltered parent fraction remained for (N)ICM and for healthy/PTSD groups. Parent fraction for all groups was 0.20 ± 0.03 by 60 minutes. Fits were prepared to describe the parent fraction of FBBG over time (**Figure S2**). Metabolic rate constants were derived according to **Equation 2** for each cohort (**Table 1**, $\tau = 7.80$ in NORM, 8.43 in PTSD, 14.47 in NICM and 10.80 in ICM; ANOVA, $p = 0.066$ NICM vs. NORM). No significant difference was found, although a trend towards significance between NORM and NICM was present ($p = 0.066$). AUCs were calculated, with significant differences between NORM and NICM revealed following an overall significant ANOVA (**Table 2**, $p = 0.048$).

Metabolite-Corrected Image-Derived Plasma Input Function

Whole blood time activity curves were sampled from regions of interest drawn in the left atrium in dynamic PET images. Subsequent data normalization, followed by corrections using **Equation 3** provided plasma input functions (**Figure 2D**). Calculations of AUC were used to compare cohorts; no significant difference existed between cardiomyopathy patients and healthy volunteers (**Table 2**).

DISCUSSION

Pharmacokinetic metrics such as plasma protein binding, metabolism and activity distribution between plasma and whole blood were determined for the radiotracer FBBG to improve accuracy of imaging quantification. From these data it can be observed that, while there are variations in metabolic profiles for clinical imaging populations, the plasma input functions of FBBG are similar among sampled cohorts. Delayed metabolism in cardiomyopathy patients may be related to reduced cardiac output and hence reduced passage through metabolic organs. Ultimately, the similarity of the parent input functions suggests a universal metabolite correction may be appropriate.

The data for the NORM cohort were subsequently compared to the first-in-human study done by Sinusas *et al*.[10] There were no significant differences found between the two groups of healthy volunteers, with a peak mean plasma concentration at 1–2 min, and clearance to 0.00078 ± 0.00083 percent of injected dose per millilitre (%ID/mL) within 5 minutes (in comparison to 0.00046 ± 0.00007 %ID/mL). Furthermore, the metabolism resembled that of the prior cohort, with parent fractions of 0.49 ± 0.11, and 0.23 ± 0.05 at 10- and 30-minutes post-injection respectively in comparison to previously reported 0.37 ± 0.19 at 15 min, and 0.19 ± 0.13 at 30 min.

This study has some limitations, namely in the collection of venous samples. Kinetic analysis of PET imaging data ideally proceeds from arterial blood activity distribution to reflect parent tracer in plasma as input to compartmental or graphical tracer kinetic models. This, however, presents a clinical obstacle due to the invasiveness of arterial blood sampling. Image-derived input functions can be deployed to arrive at similar quantification without invasive blood sampling, but lacks corrections for PBR, PF, and f_p. As demonstrated by Harms *et al.*,[14] venous blood samples can be used in quantification of HED cardiac SNS imaging, but requires an empirically derived venous-to-arterial transformation. Additionally, our study was completed across two sites with minor differences in tracer administration and blood collection protocols resulting in small timing inconsistencies in the data. These are unlikely to affect the quantitative results presented.

Finally, the limited sample size of this study may obscure additional meaningful differences in metabolism or pharmacokinetics between cohorts. The observed differences appear to be offset and minimized by rapid clearance of activity from whole blood. The resulting input functions suggest the validity of a single set of corrections for cardiomyopathy and control imaging subjects.

NEW KNOWLEDGE GAINED

Cardiomyopathy patients metabolize the sympathetic nervous system radiotracer [^{18}F]flubrobenguane more slowly than healthy control subjects. This could lead to increased radiotracer concentrations in circulating blood available for uptake into tissue and adrenergic neurons. However, [^{18}F]flubrobenguane is rapidly cleared from blood in cardiomyopathy patients, PTSD patients, and healthy subjects and therefore no statistical differences were observed in total radiotracer availability in plasma over the

course of imaging. Accurate quantification of sympathetic innervation using [^{18}F]flubrobenguane is unlikely to be confounded by metabolic differences in cardiomyopathy patients.

CONCLUSION

We assessed the pharmacokinetic and metabolic parameters of the cardiac SNS tracer [^{18}F]flubrobenguane (LMI1195) in target imaging populations. Slower tracer metabolism was observed in cardiomyopathy patients compared to healthy volunteers. FBBG clears rapidly from circulation and therefore disease-specific metabolite blood input corrections may be unnecessary given comparable distribution in plasma.

REFERENCES

(1) Yu, M.; Bozek, J.; Lamoy, M.; Guaraldi, M.; Silva, P.; Kagan, M.; Yalamanchili, P.; Onthank, D.; Mistry, M.; Lazewatsky, J.; Broekema, M.; Radeke, H.; Purohit, A.; Cdebaca, M.; Azure, M.; Cesati, R.; Casebier, D.; Robinson, S. P. Evaluation of LMI1195, a Novel ^{18}F-Labeled Cardiac Neuronal PET Imaging Agent, in Cells and Animal Models. *Circ. Cardiovasc. Imaging* **2011**, *4* (4), 435–443. https://doi.org/10.1161/circimaging.110.962126.

(2) Zelt, J. G. E.; Britt, D.; Mair, B. A.; Rotstein, B. H.; Quigley, S.; Walter, O.; Garrard, L.; Robinson, S.; Mielniczuk, L. M.; deKemp, R. A.; Beanlands, R. S. Regional Distribution of Fluorine-18-Flubrobenguane and Carbon-11-Hydroxyephedrine for Cardiac PET Imaging of Sympathetic Innervation. *JACC Cardiovasc. Imaging* **2021**, *14* (7), 1425–1436. https://doi.org/10.1016/j.jcmg.2020.09.026.

(3) Hartmann, F.; Ziegler, S.; Nekolla, S.; Hadamitzky, M.; Seyfarth, M.; Richardt, G.; Schwaiger, M. Regional Patterns of Myocardial Sympathetic Denervation in Dilated Cardiomyopathy: An Analysis Using Carbon-11 Hydroxyephedrine and Positron Emission Tomography. *Heart* **1999**, *81* (3), 262–270. https://doi.org/10.1136/hrt.81.3.262.

(4) Jacobson, A. F.; Senior, R.; Cerqueira, M. D.; Wong, N. D.; Thomas, G. S.; Lopez, V. A.; Agostini, D.; Weiland, F.; Chandna, H.; Narula, J. Myocardial Iodine-123 Meta-Iodobenzylguanidine Imaging and Cardiac Events in Heart Failure: Results of the Prospective ADMIRE-HF (AdreView Myocardial Imaging for Risk Evaluation in Heart Failure) Study. *J. Am. Coll. Cardiol.* **2010**, *55* (20), 2212–2221. https://doi.org/10.1016/j.jacc.2010.01.014.

(5) Fallavollita, J. A.; Heavey, B. M.; Luisi, A. J.; Michalek, S. M.; Baldwa, S.; Mashtare, T. L.; Hutson, A. D.; deKemp, R. A.; Haka, M. S.; Sajjad, M.; Cimato, T. R.; Curtis, A. B.; Cain, M. E.; Canty, J. M. Regional Myocardial Sympathetic Denervation Predicts the Risk of Sudden Cardiac Arrest in Ischemic Cardiomyopathy. *J. Am. Coll. Cardiol.* **2014**, *63* (2), 141–149. https://doi.org/10.1016/j.jacc.2013.07.096.

(6) Dobbeleir, A. A.; Hambÿe, A.-S. E.; Franken, P. R. Influence of High-Energy Photons on the Spectrum of Iodine-123 with Low- and Medium-Energy Collimators: Consequences for Imaging with ^{123}I-Labelled Compounds in Clinical Practice. *Eur. J. Nucl. Med.* **1999**, *26* (6), 655–658. https://doi.org/10.1007/s002590050434.

(7) Yu, M.; Bozek, J.; Lamoy, M.; Kagan, M.; Benites, P.; Onthank, D.; Robinson, S. P. LMI1195 PET Imaging in Evaluation of Regional Cardiac Sympathetic Denervation and Its Potential Role in Antiarrhythmic Drug Treatment. *Eur. J. Nucl. Med. Mol. Imaging* **2012**, *39* (12), 1910–1919. https://doi.org/10.1007/s00259-012-2204-y.

(8) Werner, R. A.; Rischpler, C.; Onthank, D.; Lapa, C.; Robinson, S.; Samnick, S.; Javadi, M.; Schwaiger, M.; Nekolla, S. G.; Higuchi, T. Retention Kinetics of the ^{18}F-Labeled Sympathetic Nerve PET Tracer LMI1195: Comparison with ^{11}C-Hydroxyephedrine and ^{123}I-MIBG. *J. Nucl. Med.* **2015**, *56* (9), 1429–1433. https://doi.org/10.2967/jnumed.115.158493.

(9) Zelt, J. G. E.; Mielniczuk, L. M.; Orlandi, C.; Robinson, S.; Hadizad, T.; Walter, O.; Garrard, L.; Beanlands, R. S. B.; deKemp, R. A. PET Imaging of Sympathetic Innervation with [^{18}F]Flurobenguan vs [^{11}C]MHED in a Patient with Ischemic Cardiomyopathy. *J. Nucl. Cardiol.* **2019**, *26* (6), 2151–2153. https://doi.org/10.1007/s12350-018-01527-5.

(10) Sinusas, A. J.; Lazewatsky, J.; Brunetti, J.; Heller, G.; Srivastava, A.; Liu, Y.-H.; Sparks, R.; Puretskiy, A.; Lin, S.; Crane, P.; Carson, R. E.; Lee, L. V. Biodistribution and Radiation Dosimetry of LMI1195: First-in-Human Study of a Novel ^{18}F-Labeled Tracer for Imaging Myocardial Innervation. *J. Nucl. Med.* **2014**, *55* (9), 1445–1451. https://doi.org/10.2967/jnumed.114.140137.

(11) Sinusas, A. J.; Liu, C. Multi-Tracer Positron Emission Tomography Quantification of Sympathetic Innervation: Tracer Similarity But Not Equivalence. *JACC Cardiovasc. Imaging* **2021**, *14* (7), 1437–1439. https://doi.org/10.1016/j.jcmg.2020.10.007.
(12) Roy, S. S.; Foraker, R. E.; Girton, R. A.; Mansfield, A. J. Posttraumatic Stress Disorder and Incident Heart Failure Among a Community-Based Sample of US Veterans. *Am. J. Public Health* **2015**, *105* (4), 757–763. https://doi.org/10.2105/ajph.2014.302342.
(13) Yu, M.; Bozek, J.; Kagan, M.; Guaraldi, M.; Silva, P.; Azure, M.; Onthank, D.; Robinson, S. P. Cardiac Retention of PET Neuronal Imaging Agent LMI1195 in Different Species: Impact of Norepinephrine Uptake-1 and -2 Transporters. *Nucl. Med. Biol.* **2013**, *40* (5), 682–688. https://doi.org/10.1016/j.nucmedbio.2013.03.003.
(14) Harms, H. J.; Huisman, M. C.; Rijnierse, M. T.; Greuter, H.; Hsieh, Y.-L.; Haan, S. de; Schuit, R. C.; Knaapen, P.; Lubberink, M.; Lammertsma, A. A. Noninvasive Quantification of Myocardial ^{11}C-*Meta*-Hydroxyephedrine Kinetics. *J. Nucl. Med.* **2016**, *57* (9), 1376–1381. https://doi.org/10.2967/jnumed.115.167437.
(15) Hilton, J.; Yokoi, F.; Dannals, R. F.; Ravert, H. T.; Szabo, Z.; Wong, D. F. Column-Switching HPLC for the Analysis of Plasma in PET Imaging Studies. *Nucl. Med. Biol.* **2000**, *27* (6), 627–630. https://doi.org/10.1016/s0969-8051(00)00125-6.

FIGURES

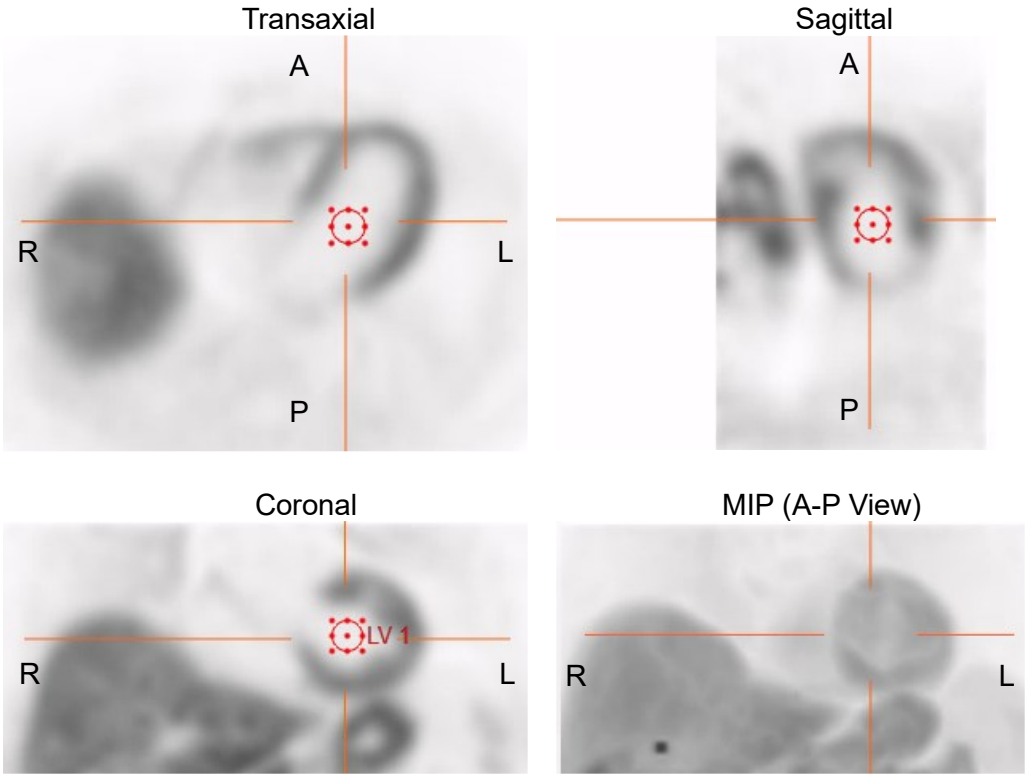

Figure 1. FBBG PET images showing tracer uptake at 30–60 minutes post-injection in a 70-year-old man with ischemic cardiomyopathy. Placement of a spherical volume-of-interest in the left ventricle (LV) cavity is illustrated in red for acquisition of the whole-blood time activity data.

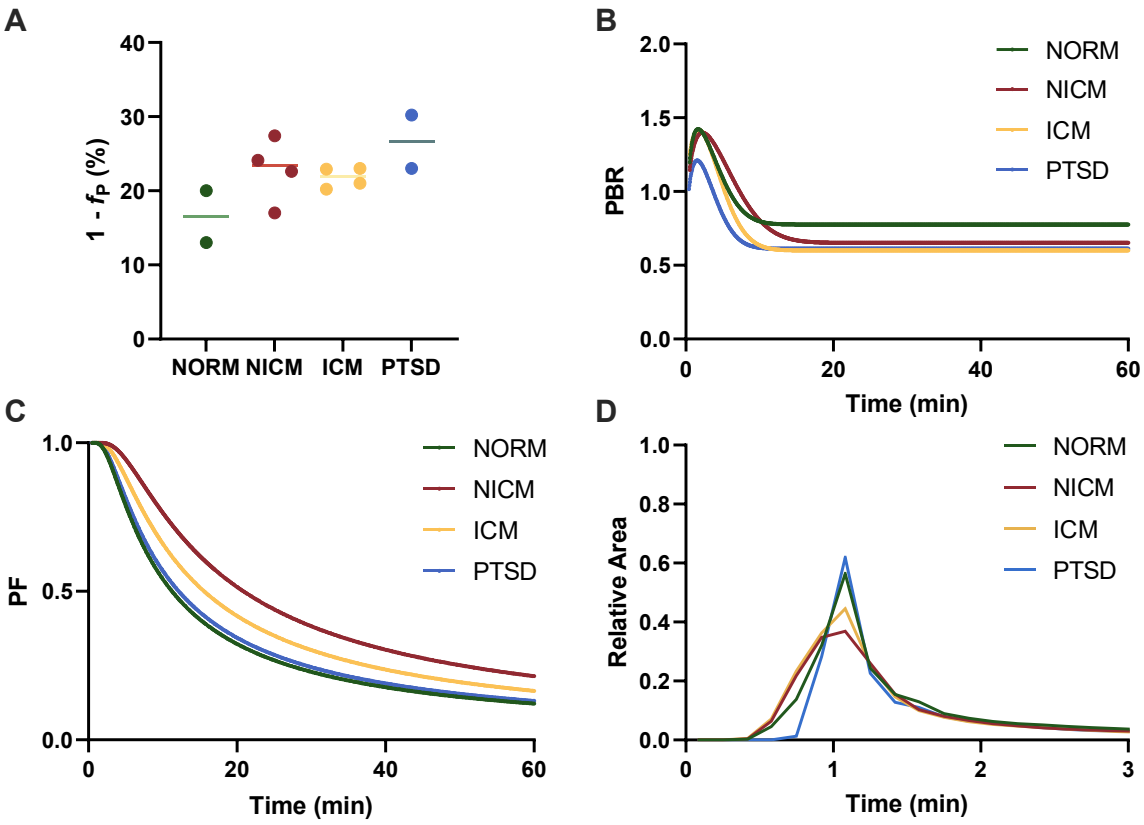

Figure 2. Metabolic and pharmacokinetic measurements. (**A**) Fraction of FBBG bound to plasma proteins (*n* = 2–4/group), (**B**) plasma-to-whole blood ratio of radioactivity following i.v. administration of FBBG (*n* = 5/group), (**C**) fraction of parent FBBG, 0–60 minutes (*n* = 5/group), (**D**) parent plasma input function time activity curves, 0–3 minutes (*n* = 5/group).

TABLES

Table 1. Fitted function parameters for plasma-to-blood ratio (PBR) and parent fraction (PF)

	PBR				PF
	A	***B***	***m*** **(min^{-2})**	***n*** **(min^{-1})**	**τ (min)**
NORM	0.86 ± 0.13	0.75 ± 0.10	0.06 ± 0.06	1.71 ± 1.30	7.99 ± 1.57
NICM	0.92 ± 0.04	0.63 ± 0.20	0.02 ± 0.01	1.06 ± 0.40	15.87 ± 8.42
ICM	0.90 ± 0.09	0.61 ± 0.05	0.03 ± 0.01	1.92 ± 1.63*	10.81 ± 1.95
PTSD	0.85 ± 0.16	0.69 ± 0.04	0.12 ± 0.16	1.37 ± 0.87	8.80 ± 2.70
ANOVA	p = 0.762	p = 0.275	p = 0.281	p = 0.278	p = 0.063

Values are mean ± standard deviation; * p < 0.05 vs. NORM

Table 2. Area under the curve analyses of PBR, PF, and C_{FP}

	$AUC_{PBR(t)}$	$AUC_{PF(t)}$	$AUC_{C_{FP}(t)}$
NORM	48.66 ± 3.12	19.41 ± 2.36	0.62 ± 0.08
NICM	42.53 ± 10.98	28.06 ± 7.78*	0.61 ± 0.04
ICM	40.36 ± 3.31	23.43 ± 2.60	0.56 ± 0.06
PTSD	42.33 ± 3.91	20.52 ± 4.19	0.55 ± 0.09
ANOVA	p = 0.217	p = 0.048	p = 0.333

Values calculated 0–60 min, mean ± standard deviation;
* p < 0.05 vs. NORM

SUPPLEMENTAL INFORMATION

PTSD Recruitment:

Individuals with PTSD are veterans or members of the Canadian Armed Forces with a history of military-related trauma recruited from the Operational Stress Injury clinic at the Royal Ottawa Mental Health Centre. The Mini International Neuropsychiatric Interview as well as the Clinician Administered PTSD Scale and the Life Events Checklist for DSM-5 were administered by a trained psychiatrist to confirm a PTSD diagnosis.[16] This study was approved by the Royal Ottawa Health Care Group Research Ethics Board (#2018035).

Plasma Protein Binding:

Patient plasma was obtained through centrifugation (3200 RPM at 4 °C for 7 minutes) of a blood sample collected prior to tracer administration. Around 750 kBq of FBBG was added to a 500 μL aliquot of plasma, which was then incubated for 10 minutes at 37 °C. Approximately 400 μL of the spiked plasma was loaded into the upper level of a Millipore ultrafiltration tube (Centrifree®) with a 30,000 Da molecular weight cut-off. The remaining 100 μL was used to aliquot precisely measured volumes (20 μL) into 3 counting tubes. The filtration devices were then centrifuged for 10 minutes at 3200 RPM. Once complete, the filtrate was aliquoted (20 μL) into 3 additional counting tubes. The counting tubes were placed into a rack and activity was measured on a Hidex AMG gamma counter. Triplicates were then averaged to determine the plasma protein binding for each imaging subject.

Plasma-to-Whole Blood Ratio

500 μL of whole blood was sampled from each timepoint. The blood vials were then centrifuged to isolate plasma, from which 500 μL was collected. The aliquots were then placed on the γ-counter to determine their counts. At each timepoint, the ratio of activity in the plasma was then compared to the whole blood to determine PBR.

HPLC Metabolites:

Whole blood samples drawn during PET were centrifuged to isolate plasma. Plasma samples were mixed with urea (1 g) and then diluted to 2 mL with water. They were then co-injected with unlabeled FBBG on to a column-switching radio-HPLC[15] equipped with a Waters OASIS HLB capture column and a Luna 10 μm C18 100 Å analytic column (250 × 4.60 mm). The capture column was eluted with 1% MeCN/H_2O for 4 minutes prior to valve-switching, at which point the capture column was eluted in reverse direction and in line with the analytical column using 27.5% MeCN/0.1 M ammonium formate buffer. Flow rates were 1 mL/min. The compound retention was ~16 min and was confirmed by monitoring the UV chromatogram. A fraction collector was used to gather the eluate with 2 min resolution, then assayed for activity on a γ-counter. Polar metabolites were summed and compared to the parent compound to determine the fraction of FBBG.

SUPPLEMENTAL FIGURES

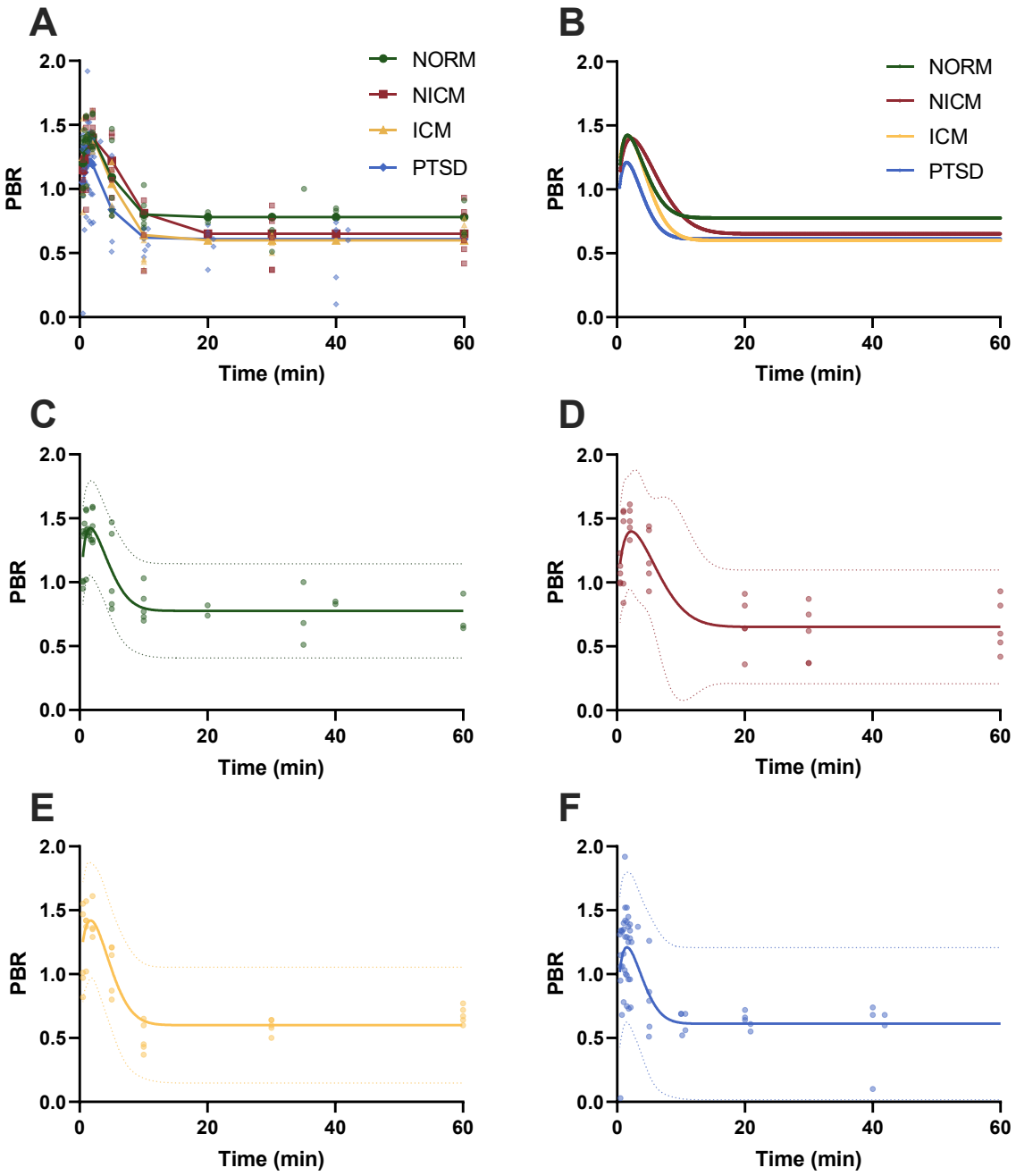

Figure S1. Plasma-to-whole blood ratio, mean and 95% CI. (A) Measured PBR data, (B) PBR fitted functions, (C) NORM, (D) NICM, (E) ICM, (F) PTSD

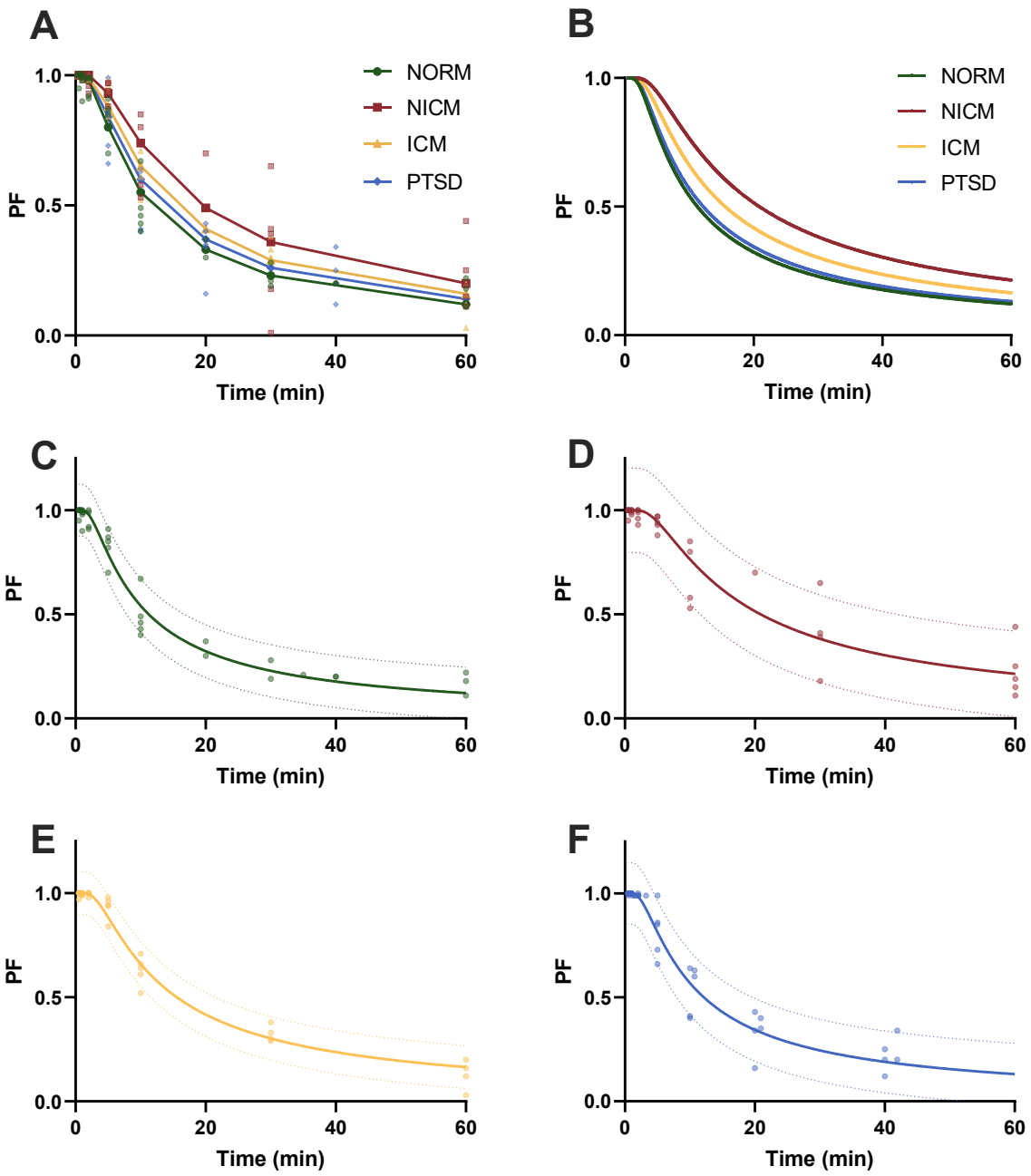

Figure S2. Parent fraction, mean and 95% CI. (A) Measured PF data, (B) PF fitted functions, (C) NORM, (D) NICM, (E) ICM, (F) PTSD

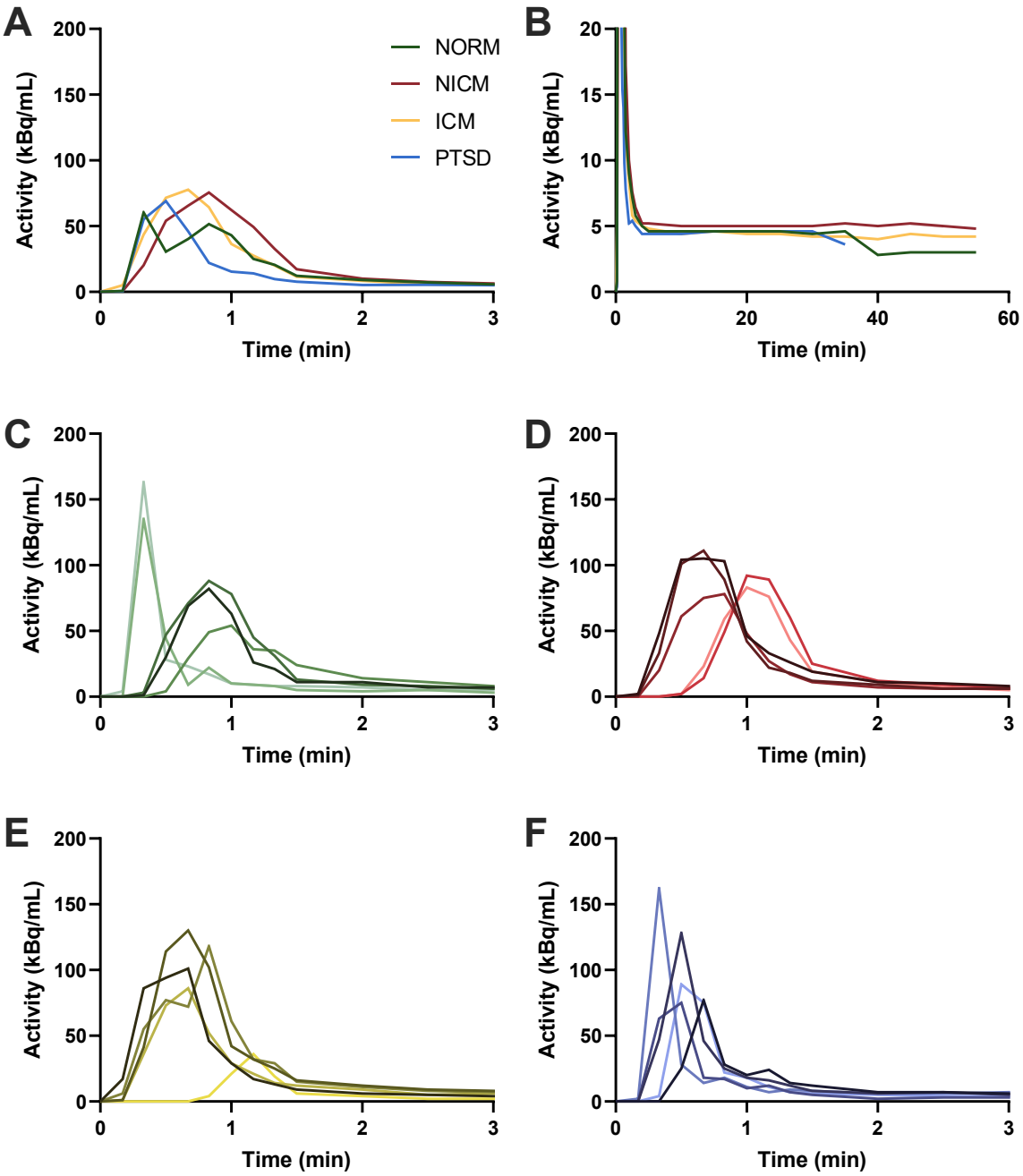

Figure S3. Left atrial time-activity curves. Full cohort (A) 0–3 minutes; (B) 0–60 minutes. (C) NORM, (D) NICM, (E) ICM, (F) PTSD

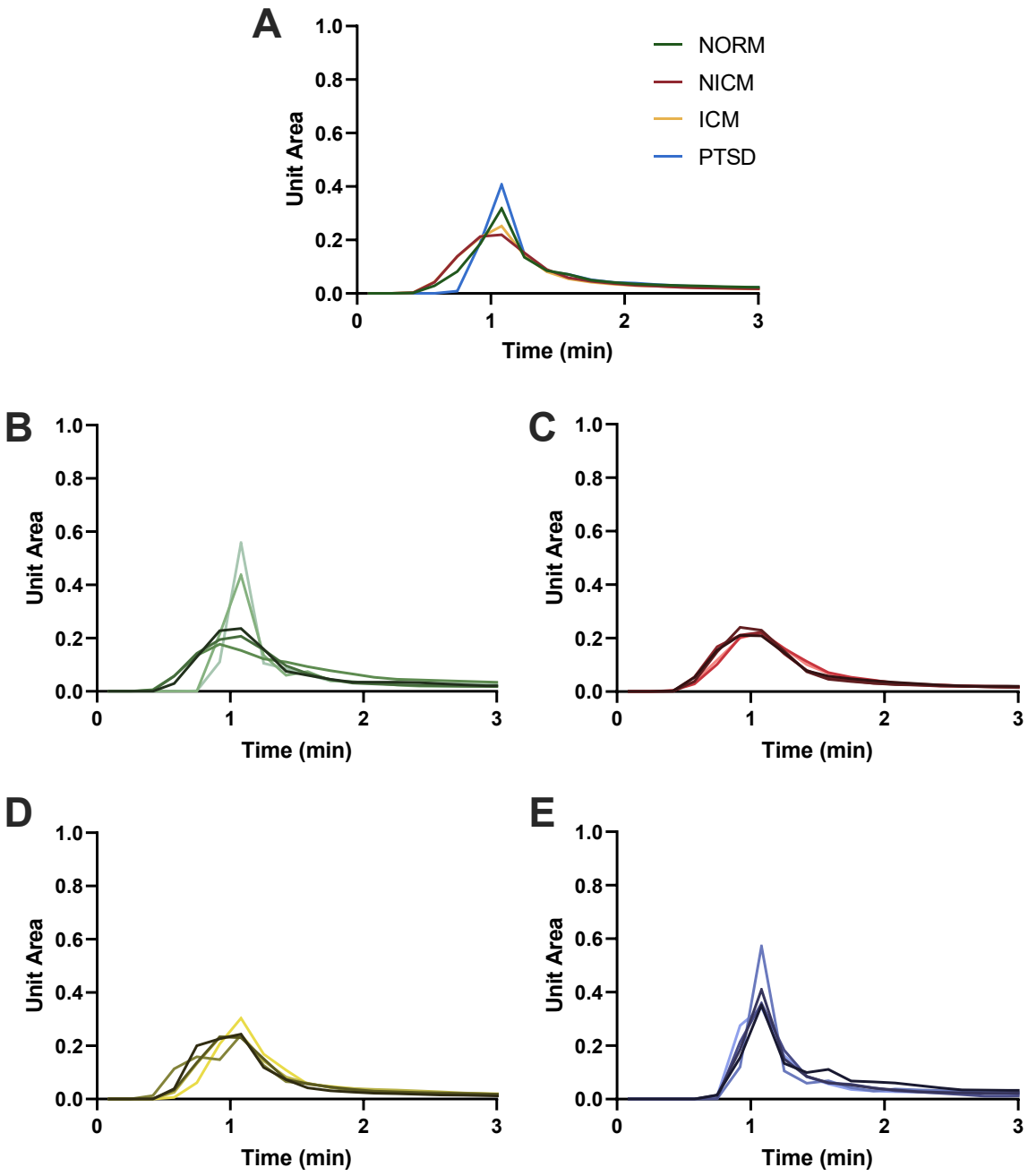

Figure S4. Left atrial cavity time-activity curves normalized by gamma variate. (A) Full cohort, (B) NORM, (C) NICM, (D) ICM, (E) PTSD

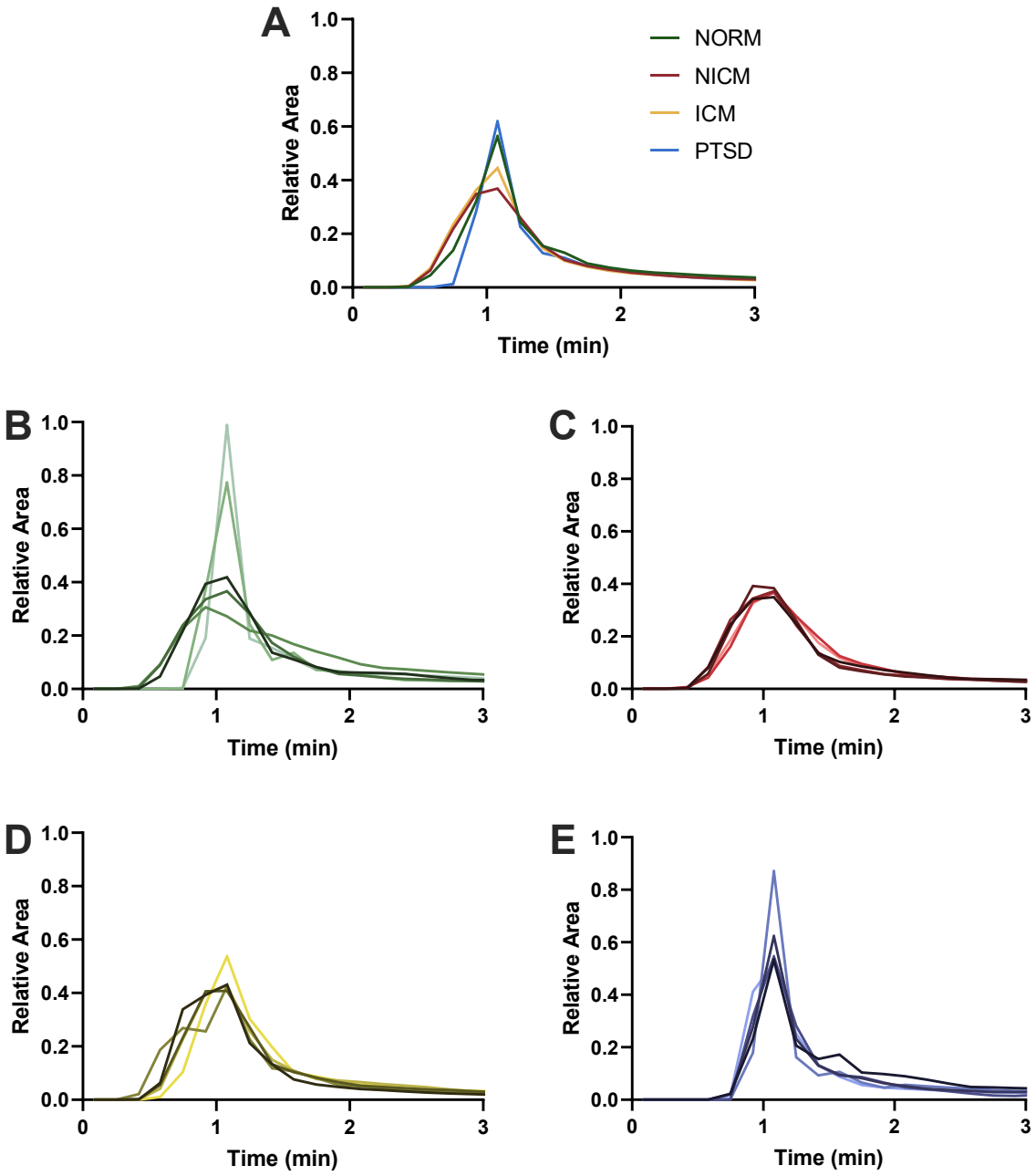

Figure S5. Parent plasma input function time-activity curves after data normalization and formula correction. (A) Full cohort, (B) NORM, (C) NICM, (D) ICM, (E) PTSD

SUPPLEMENTAL TABLE

Table S1. Characteristics of imaging subjects

	NORM *n* = 5	**NICM** *n* = 5	**ICM** *n* = 5	**PTSD** *n* = 5
Clinical Data				
Male	5 (100)	3 (60)	5 (100)	3 (60)
Age (yrs)	51.0 ± 7.8	62.4 ± 4.3	68.0 ± 6.5	46.4 ± 5.6
Caucasian	2 (40)	2 (40)	5 (100)	-
BMI (kg/m^2)	27.2 ± 3.5	28.8 ± 5.4	30.6 ± 3.3	28.8 ± 3.1
NYHA class (I/II/III/IV)	0/0/0/0	1/3/0/0	2/2/0/0	0/0/0/0
Heart rate (min^{-1})	62.6 ± 8.3	65.8 ± 13.5	58.2 ± 3.5	70.0 ± 11.1
Systolic blood pressure (mmHg)	131.6 ± 11.1	131.2 ± 22.6	133.6 ± 16.3	124.4 ± 14.6
Imaging data				
FFBG Dose (MBq)	257.9 ± 37.9	276.4 ± 51.8	293.6 ± 19.6	257.6 ± 28.7
LVEF (%)	60.2 ± 5.6	39.8 ± 6.9	33.5 ± 8.0	62.4 ± 7.0
Laboratory data				
NT-proBNP (pg/mL)	<50	392.6 ± 443.8	428.6 ± 319.2	67.3 ± 5.1
Creatinine (μM)	88.3 ± 15.0	80.2 ± 22.5	106.6 ± 48.1	80.5 ± 22.6
Medications				
β-blockers	0 (0)	5 (100)	5 (100)	0 (0)
ACE/ARB	0 (0)	2 (40)	1 (20)	0 (0)
Diuretics	0 (0)	1 (20)	3 (60)	0 (0)
Lipid lowering agents	1 (20)	4 (80)	5 (100)	1 (20)

Values are *n* (%) or mean ± standard deviation

SUPPLEMENTAL REFERENCES

16. Sheehan DV, Lecrubier Y, Sheehan KH, et al. The Mini-International Neuropsychiatric Interview (M.I.N.I.): The Development and Validation of a Structured Diagnostic Psychiatric Interview for DSM-IV and ICD-10. *J Clin Psychiatry* **1998**;*59*(S20):22–33.